RESEARCH ARTICLE

≬ ISEV

Rapid and efficient isolation platform for plasma extracellular vesicles: EV-FISHER

Wei-Lun Pan[1,2] | Jun-Jie Feng[1] | Ting-Ting Luo[1] | Yong Tan[2] | Bo Situ[1] |
Rienk Nieuwland[3] | Jing-Yun Guo[4] | Chun-Chen Liu[1] | Han Zhang[1] | Jing Chen[1] |
Wen-Hua Zhang[5] | Jun Chen[2] | Xian-Hua Chen[6] | Hong-Yue Chen[2] | Lei Zheng[1] 🔟 |
Jin-Xiang Chen[2] | Bo Li[1]

[1]Department of Laboratory Medicine, Nanfang Hospital, Southern Medical University, Guangzhou, China

[2]Guangdong Provincial Key Laboratory of New Drug Screening, School of Pharmaceutical Sciences, Southern Medical University, Guangzhou, China

[3]Laboratory of Experimental Clinical Chemistry, Vesicle Observation Centre, Amsterdam University Medical Center, Amsterdam, The Netherlands

[4]Breast Center, Department of General Surgery, Nanfang Hospital, Southern Medical University, Guangzhou, China

[5]College of Chemistry, Chemical Engineering and Materials Science, Soochow University, Suzhou, China

[6]Department of Clinical Laboratory, Liuzhou Municipal Liutie Central Hospital, Liuzhou, China

Correspondence
Bo Li, Department of Laboratory Medicine, Nanfang Hospital, Southern Medical University, Guangzhou 510515, China.
Email: nfyylibo2012@smu.edu.cn

Jin-Xiang Chen, Guangdong Provincial Key Laboratory of New Drug Screening, School of Pharmaceutical Sciences, Southern Medical University, Guangzhou 510515, China.
Email: jxchen@smu.edu.cn

Lei Zheng, Department of Laboratory Medicine, Nanfang Hospital, Southern Medical University, Guangzhou 510515, China.
Email: nfyyzhenglei@smu.edu.cn

Abstract

Extracellular vesicles (EVs) have found diverse applications in clinical theranostics. However, the current techniques to isolate plasma EVs suffer from burdensome procedures and limited yield. Herein, we report a rapid and efficient EV isolation platform, namely, EV-FISHER, constructed from the metal-organic framework featuring cleavable lipid probes (PO_4^{3-}-spacer-DNA-cholesterol, PSDC). The EV-FISHER baits EVs from plasma by cholesterol and separates them with an ordinary centrifuge. The captured EVs could be released and collected upon subsequent cleavage of PSDC by deoxyribonuclease I. We conclude that EV-FISHER dramatically outperforms the ultracentrifugation (UC) in terms of time (∼40 min vs. 240 min), isolation efficiency (74.2% vs. 18.1%), and isolation requirement (12,800 g vs. 135,000 g). In addition to the stable performance in plasma, EV-FISHER also exhibited excellent compatibility with downstream single-EV flow cytometry, enabling the identification of glypican-1 (GPC-1) EVs for early diagnosis, clinical stages differentiation, and therapeutic efficacy evaluation in breast cancer cohorts. This work portrays an efficient strategy to isolate EVs from complicated biological fluids with promising potential to facilitate EVs-based theranostics.

Abbreviations: Acronym, Full English description; AFM, Atomic force microscopy; BC, Breast cancer patients; BC-T, Breast cancer patients after treatments; CHO, Cholesterol; Cy5, Cyanine 5; DLS, Dynamic light scattering; DMEM, Dulbecco's Modified Eagle Medium; DMF, N, N-Dimethylformamide; DNase I, Deoxyribonuclease I; EDX, Energy dispersive X-ray; EV-FISHER, Extracellular Vesicles Fisher; EVs, Extracellular vesicles; FBS, Fetal bovine serum; FITC, Fluorescein isothiocyanate; GPC-1, Glypican-1; HD, Healthy donors; HEPES, 4-(2-Hydroxyethyl)-1-piperazine ethane sulfonic acid; ICP-MS, Inductively coupled plasma mass spectrometry; LMCT, Ligand to metal charge transfer; MEA, Cysteamine; MISEV, Minimal Information for Studies of Extracellular Vesicles; MOFs, Metal-organic frameworks; NaCl, Sodium chloride; nFCM, Nano flow cytometer; NH_2-BDC, 2-Amino-1,4-benzendicarboxylic acid; NTA, Nanoparticle tracking analysis; PBS, Phosphate buffer saline; PFP, Platelet-free plasma; PSDC, PO_4^{3-}-spacer-DNA-cholesterol; PXRD, Powder X-ray diffraction; RPMI 1640, Roswell Park Memorial Institute 1640; SDS-PAGE, Sodium dodecyl sulfate-polyacrylamide gel electrophoresis; SEC, Size exclusion chromatography; TEM, Transmission electron microscopy; UC, Ultracentrifugation; UV-Vis, Ultraviolet-visible; XPS, X-ray photoelectron spectroscopy; $ZrOCl_2 \cdot 8H_2O$, Zirconium(IV) chloride oxide octahydrate.

- - - - - - - -

1 | INTRODUCTION

Extracellular vesicles (EVs) are phospholipid-bilayer-surrounded particles ranging from 30 to 1000 nm released by all types of cells in an evolutionarily conserved manner (Liang et al., 2021). Increasing evidence has suggested that EVs play vital roles in intercellular communication, disease development and progression (Wiklander et al., 2019; Xie et al., 2019; Xu et al., 2018,). In particular, EVs carry abundant biomolecules such as proteins, nucleic acids, lipids etc., which have excellent potential as next-generation biomarkers (Vasconcelos et al., 2019; Wang et al., 2018). For example, glypican-1 (GPC-1) positive EVs were overexpressed in breast cancer, exhibiting excellent performance in early diagnosis and therapeutic efficacy monitoring (Melo et al., 2015). However, EVs with heterogeneous sizes are present in biological fluids, *for example*, plasma, serum, urine, and saliva, wherein non-EV biomolecules are dominant. It is thus a formidable challenge to develop an efficient method to isolate EVs from complex fluids, such as plasma.

At the current stage, differential ultracentrifugation (UC) is the most commonly used method for isolating EVs from plasma. However, UC is time-consuming and co-isolates contaminants such as protein aggregates (Boriachek et al., 2018). Therefore, alternative methods such as asymmetric flow field-flow fractionation (Zhang & Lyden, 2019), capillary-channelled polymer fibre-based chromatographic method (Jackson et al., 2021), exosome detection via the ultrafast-isolation system: EXODUS (Chen et al., 2021), size exclusion chromatography (SEC) (Oeyen et al., 2018), ultrafiltration (Woo et al., 2017), polymeric precipitation (Doyle & Wang, 2019), and immunoaffinity (Choi et al., 2022; Zhu et al., 2021), have also been proposed to isolate EVs for varied downstream applications with different merits and limitations, which summarized in Table S1. Nevertheless, it remains a challenge to isolate plasma EVs with preferable yield in a clinical-friendly manner.

Recently, a lipid nanoprobe has been developed to target the phospholipid bilayer of EVs to facilitate their isolation (Wan et al., 2017). Compared to the traditional EVs recognition elements like antibodies, peptides, and aptamers, the lipid nanoprobe captures EVs by targeting EV's phospholipid bilayer rather than the specific surface biomacromolecules (CD63, CD9, phos-phatidylserine, etc.) (Koliha et al., 2016; Zhang et al., 2021; Zhao et al., 2016). In addition, the strong hydrophobic interaction of the lipid probe and EVs membrane promises an efficient binding. Therefore, this lipid-based strategy proposes its superiority in isolating the total EV population and thus provides comprehensive sample information for clinical judgment.

Metal-organic frameworks (MOFs), supported by principally unlimited permutations of metal ions and organic ligands, have emerged as promising materials for diverse applications (Hu et al., 2018; Wang et al., 2019; Zhao et al., 2018). Concerning nanomedicine, MOFs have been widely used as carriers or substrates for theranostic applications (Deng et al., 2019; Wu et al., 2018; Zhang et al., 2016). The adjustable pore size, extraordinary surface area, and abundant diversity of structure entitle MOFs to separate small molecules (e.g., gas, peptides, ions), yet the development of MOFs for macromolecule separation is still challenging (Lin et al., 2019; Wu et al., 2021; Zhang et al., 2017). Recently, an antibodies-assisted MOF platform has been developed for EV isolation, named Tim4@ILI-01 (Zhang et al., 2021). Yet this strategy still requires laborious modification and a long isolation time (> 2 h). Therefore, a rapid and efficient EV isolation platform based on MOFs remained largely unexplored.

Herein, we report a MOF platform termed EV-FISHER for the rapid enrichment and isolation of EVs. EV-FISHER is constructed from defected Zirconium (Zr)-based MOF of UiO-66-NH$_2$ hybridized with cleavable lipid probes PO$_4^{3-}$-spacer-DNA-cholesterol (PSDC). As demonstrated in Figure 1(a), the UiO-66-NH$_2$ is first activated to acquire the defect structure, which provides it with more abundant modification sites. Next, the defected UiO-66-NH$_2$ is readily associated with PSDC through PO$_4^{3-}$-Zr(IV) (Ji et al., 2018) to form EV-FISHER (PSDC@MOF), ensuring a simple and high-affinity connection (Liu et al., 2014). Consequently, MOF UiO-66-NH$_2$ acts as the 'handle' to bind with the 'fishing line' PSDC.

As illustrated in Figure 1(b) and Table S2, the EV-FISHER 'baits' EVs from plasma with cholesterol and enriches them via low-speed centrifugation. Subsequently, deoxyribonuclease I (DNase I) is added to hydrolyse the DNA in PSDC to detach EVs.
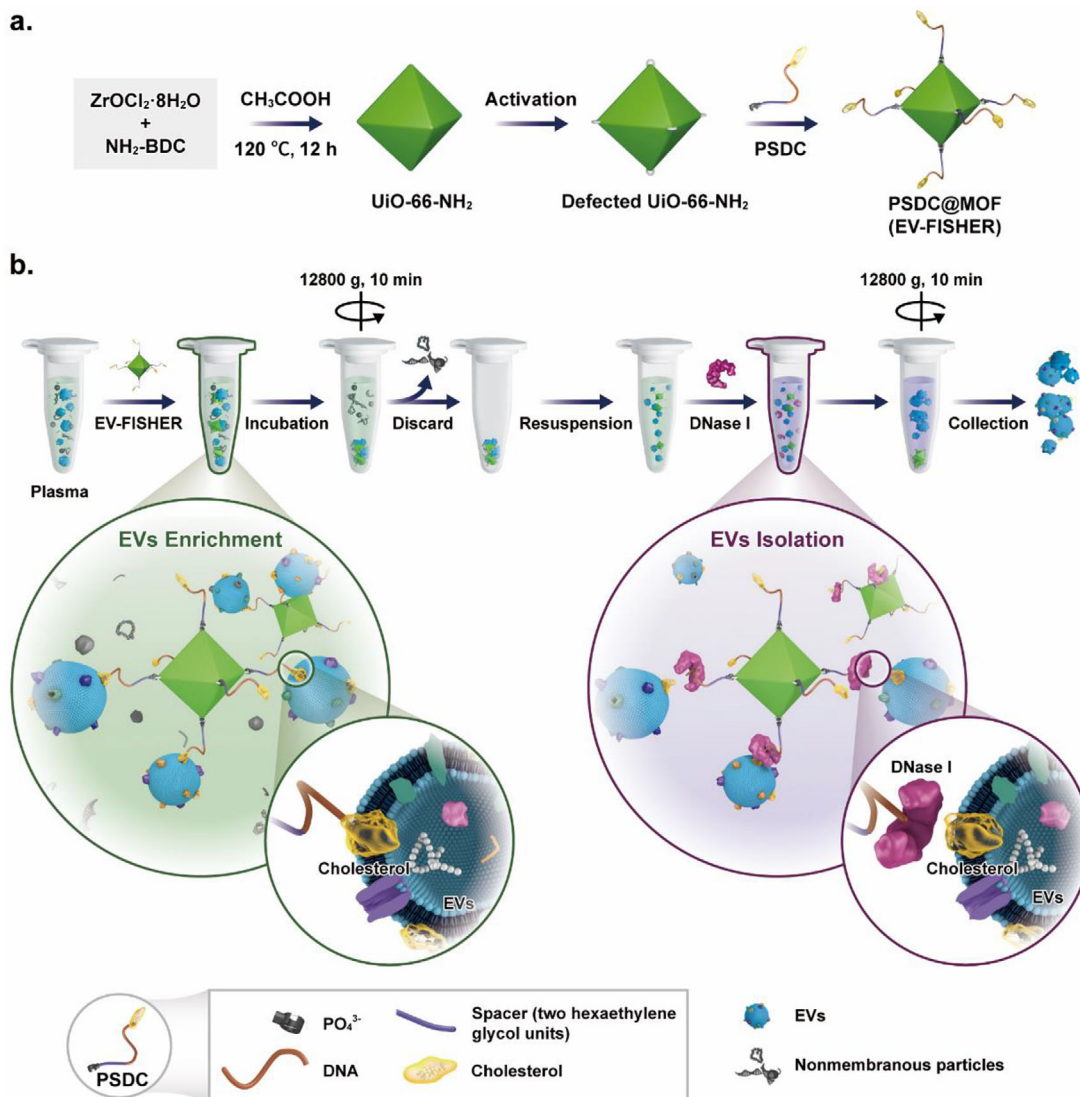
FIGURE 1 Schematic illustration of (a) the synthesis of EV-FISHER and (b) the workflow of plasma EVs isolation

Finally, purified EVs can be obtained after removing the MOF segment. The high affinity of cholesterol toward EVs' membrane coupled with the advantages of MOF entitled EV-FISHER to outperform the UC method in terms of time (~40 min *vs.* 240 min), isolation efficiency (74.2% *vs.* 18.1%), and isolation requirement (12 800 g *vs.* 135 000 g). This work presents a promising strategy for fast and efficient plasma EVs isolation in general clinical laboratories for downstream analysis.

2 | MATERIALS AND METHODS

2.1 | Chemicals and materials

Zirconium(IV) chloride oxide octahydrate ($ZrOCl_2 \cdot 8H_2O$, #Z820694), 2-Amino-1,4-benzendicarboxylic acid (NH_2-BDC, #10312-55-7), Hoechst 33258 (#B860511), and poly-L-lysine (#P856789) were purchased from Macklin. N, N-Dimethylformamide (DMF, AR, 99.5%), ethanol absolute (AR, 99.7%), and acetic acid (AR, 99.5%) were obtained from Guangdong Guanghua Sci-Tech. Glucose oxidase (#G2133), catalase (#C40), cysteamine (MEA, #30070), Tris base (#T1503), D-(+)-Glucose (#G7528), DNase I (#D5025), cholesterol (CHO, #C8667) and PKH67 Green Fluorescent Cell Linker Midi Kit (PKH67, #MIDI67) were supplied by Sigma-Aldrich. Sodium chloride (NaCl, #C111533) was bought from Aladdin. 4-(2-Hydroxyethyl)-1-piperazine ethane sulfonic acid (HEPES, #H1095) was purchased from Solarbio. Hydrogen chloride (#C06808852) was purchased from Nanjing Reagent. Dulbecco's Modified Eagle Medium (DMEM), Roswell Park Memorial Institute 1640 (RPMI 1640), foetal bovine serum (FBS), penicillin-streptomycin, and phosphate buffer saline (PBS, 1×, pH 7.4) were purchased from Gibco. Antibodies CD63

(#510953), CD9 (#380441), glypican-1 (GPC-1, #R22799) and TSG101 (#R25999) were obtained from ZEN BIO. Goat anti-rabbit IgG/FITC antibody (#bs-0295G-FITC), goat anti-rabbit IgG/Alexa Fluor 647 antibody (#bs-0295G-AF647) and goat anti-rabbit IgG/gold antibody (#bs-0295G-Gold) were brought from Bioss. DNA sequences used in the paper were obtained from Sangon Biotech and listed in Table S3. All the materials were used as received without further purification. Ultrapure water was obtained from a PURELAB Classic system (ELGA LabWater).

2.2 | Synthesis of UiO-66-NH2

UiO-66-NH$_2$ was synthesized according to the previous reports (Chen et al., 2019; Wang et al., 2017) with slight modification. The solution of ZrOCl$_2$·8H$_2$O (20 mg, 62.1 μmol) in DMF (5 ml) was added to a vial containing DMF (7 ml) and acetic acid (1.5 ml), after which the solution of NH$_2$-BDC (11.7 mg, 64.6 μmol) in DMF (3 ml) was injected into the vial. Then the mixture was sonicated for 20 min and stayed at 120°C for 12 h to produce UiO-66-NH$_2$ nanoparticles. The resulting powder was collected by centrifugation (12 800 g, 10 min), and washed with ethanol three times before drying at 80°C under reduced pressure for activation.

2.3 | Synthesis of EV-FISHER

The activated UiO-66-NH$_2$ powder (10 mg) was dispersed in ultrapure water (25 ml) containing PSDC (2.8 μM). The mixture was left on a shaker for 12 h incubation at room temperature, and NaCl solution was slowly added to reach a concentration of 0.5 M. The formed EV-FISHER (PSDC@MOF) was finally collected by centrifugation (12 800 g, 10 min) and washed with ultrapure water five times to remove unbound PSDC. Finally, the EV-FISHER was re-dispersed in HEPES buffer (25 mM HEPES, 100 mM NaCl) and stored at 4°C for further use.

2.4 | Preparation of model EVs

Breast cancer cells MDA-MD-231 were cultured in DMEM containing 10% FBS and 1% antibiotics (penicillin-streptomycin, 10 000 U/ml) with 5% CO$_2$ in air at 37°C. The cells were washed with PBS when they reached 70% coverage and further cultured in DMEM for 12 h. After that, cells were rewashed with PBS and cultured for 48 h in DMEM containing 1% EVs depleted FBS. Cell supernatant was then harvested and centrifuged at 300 g, 2000 g, and 10 000 g, respectively, for the removal of dead cells and cell debris. The resulting cell medium was centrifuged under 135 000 g for 70 min (SW 32 Ti Swinging-Bucket Rotor, Beckman), and the precipitate was resuspended with HEPES buffer. This ultracentrifugation procedure was repeated. The resulting pellet (model EVs) was collected and stored at -80°C for further use.

2.5 | Characterization of lipid probe on MDA-MB-231 cells by confocal microscopy

Breast cancer cells MDA-MB-231 were seeded in glass culture dishes with proper cell density. The cells were washed with PBS, and then DMEM containing Cy5-DNA-CHO (10 nM) or Cy5-DNA (10 nM) were added for 2 h incubation with 5% CO$_2$ in air at 37°C. After that, cells were washed with PBS followed by stained with nuclear dye Hoechst 33258 for 10 min before observation (LSM 880, Carl Zeiss). The samples were observed with the excitation of 405 nm for Hoechst 33258 and 633 nm for Cy5.

2.6 | Characterization of lipid probe on model EVs by super-resolution microscopy

The glass culture dishes were first activated by poly-L-lysine (1 mg/ml, 100 μl) for 30 min at room temperature. Then, model EVs from MDA-MB-231 cells (10^9 particles, 250 μl) were seeded in activated culture dishes for 30 min of absorption. Excess EVs were removed by HEPES buffer, after which Cy5-DNA-CHO (10 nM) was added for 30 min incubation. Unbound Cy5-DNA-CHO was washed away by HEPES buffer, and EVs@Cy5-DNA-CHO complexes were further stained with membrane dye PKH67 (0.5 μl of the PKH67 ethanolic dye solution + 250 μl of the Diluent C) for 3 min in the dark. Next, the dye was removed, and the sample was washed with HEPES buffer five times. Finally, the dishes were covered with the imaging buffer (see more details in Supporting Information) for observation (Nikon N-STORM). Lasers with 488 and 647 nm wavelengths were selected for dye PKH67 and Cy5, respectively. Each channel was set to collect 10 000 images for analysis.

2.7 | Isolation of model EVs by EV-FISHER

2.7.1 | Enrichment of model EVs

The model EVs with 8×10^8/ml were incubated with EV-FISHER (0.4 mg/ml, 500 μl) for 10 min on a HulaMixer® Sample Mixer at room temperature. Next, the samples were centrifuged (12 800 g, 10 min) and suspended in HEPES buffer to obtain EVs@EV-FISHER complexes.

For transmission electron microscopy (TEM, Hitachi H-7500) imaging, the EVs@EV-FISHER solution was added to a copper grid for fixation and stained with 2% phosphotungstic acid for 5 min. The excess solution was removed with filter paper carefully. Finally, the samples were dried at room temperature naturally before observation.

For atomic force microscopy (AFM, Bruker) scanning, the EVs@EV-FISHER solution was dropped on a mica sheet for fixation, followed by carefully drying the mica sheet before scanning.

2.7.2 | Release of model EVs

DNase I (25 Units) dissolved in cleavage buffer (HEPES buffer, 2.5 mM Mg^{2+}, 0.5 mM Ca^{2+}) was added to EVs@EV-FISHER complexes to release the captured EVs. The released EVs in the supernatant was collected after centrifugation (12 800 g, 10 min).

2.8 | Calculation of isolation efficiency by nanoparticle tracking analysis (NTA)

The isolation efficiency (recovery rate) was defined as R = Nr/N, in which Nr represented the particle number recovered by EV-FISHER and N denoted the particle number of model EVs used as the source material.

2.9 | Characterization of model EVs membrane proteins by super-resolution microscopy

The isolated model EVs by EV-FISHER were absorbed on a poly-L-lysine (1 mg/ml, 100 μl) activated culture glass dish for 30 min, and excess EVs were washed away by HEPES buffer. Then EVs were stained with dye PKH67 (0.5 μl of the PKH67 ethanolic dye solution + 250 μl of the Diluent C) for 3 min in the dark. Next, the dye was washed away with HEPES buffer five times. Further, the EVs were labelled with antibodies CD63, CD9, and GPC-1 (1:100), respectively, followed by Alexa Fluor 647 second antibody (1:100). The labelled EVs were covered by the imaging buffer (see more details in Supporting Information) for observation (Nikon N-STORM). Samples were excited with 488 nm for dye PKH67 and 647 nm for Alexa Fluor 647 fluorescent antibody, respectively. Each channel was set to collect 10 000 images for analysis.

2.10 | Plasma collection and storage

The blood samples were collected by anti-coagulant tubes with the addition of dipotassium ethylene diamine tetraacetate (EDTA-2K, AOSAITE Medical Devices Co., Ltd.). After the blood was drawn from patients or healthy donors, they were centrifuged (1200 g, 5 min) to obtain the plasma within 2 h. Afterwards, the plasma samples were centrifuged (2500 g, 15 min) twice to remove the platelet and collect the platelet-free plasma (PFP) in the supernatant. The PFP samples were stored at -80°C for further use.

2.11 | Isolation of plasma EVs by EV-FISHER

The PFP (1 ml) was diluted to 3 ml with HEPES buffer before incubated with EV-FISHER (0.4 mg/ml, 1 ml) on a HulaMixer® Sample Mixer at room temperature. Next, the samples were centrifuged (12 800 g, 10 min) and washed with HEPES buffer to obtain EVs@EV-FISHER complexes. Then, DNase I (50 Units) dissolved in cleavage buffer (HEPES buffer, 2.5 mM Mg^{2+}, 0.5 mM Ca^{2+}) was added to EVs@EV-FISHER complexes to release the captured EVs. Finally, the released EVs were collected in the supernatant after centrifugation (12 800 g, 10 min). All the plasma samples were obtained from Nanfang Hospital, Southern Medical University, with approval (NFEC-201512-K2).

2.12 | Isolation of plasma EVs by UC

The PFP (1 ml) was diluted to 4 ml with PBS, followed by centrifugation (135 000 g, 70 min). Next, the obtained precipitation was suspended by PBS and subjected to the second round of centrifugation (135 000 g, 70 min). Finally, the sediment (EVs) was collected with PBS.

2.13 | Isolation of plasma EVs by SEC

The isolation of plasma EVs by SEC was achieved using the EV isolation kit (qEVoriginal Size Exclusion Columns, Izon) according to the instructions. Briefly, the column was attached upright and flushed with 10 ml PBS. Subsequently, the PFP (500 μl) was loaded onto the loading frit and run into the column, followed by elution with PBS. Finally, the EV component was collected in a fraction from 2.5 to 4 ml of elution.

2.14 | GPC-1 EVs detection by nano flow cytometer (nFCM)

The PFP (150 μl) were incubated with EV-FISHER (0.4 mg/ml, 500 μl) for 10 min on a HulaMixer® Sample Mixer at room temperature. Next, the samples were centrifuged (12 800 g, 10 min) and washed with HEPES buffer to obtain EVs@EV-FISHER complexes. Antibody GPC-1 (1:500) was introduced in the EVs@EV-FISHER for 30 min to label the captured EVs. Then the GPC-1@EVs@EV-FISHER complexes were washed and further labelled with a second antibody (FITC) for 30 min. Next, the samples were washed and treated with DNase I (25 Units) to release the labelled EVs. Finally, the labelled EVs were collected by centrifugation (12 800 g, 10 min) for nFCM analysis.

The nano flow cytometer was purchased from Xiamen NANOFCM. Before the measurement, the flow cytometer system was purged with company-equipped wash buffer and ultrapure water and calibrated according to instructions (Tian et al., 2018). Then, the EV samples (100 μl) were loaded on the flow cytometer for analysis (FITC fluorescent channel).

2.15 | Statistical analysis

Statistical analysis was performed using Student's two-tailed t-tests in Graph Prism 8 (GraphPad Software, CA) to determine significant differences. The data are presented as mean $\pm$ standard error of the mean of at least three independent experiments. $P < 0.05$ was considered statistically significant.

3 | RESULTS

3.1 | Synthesis and characterization of EV-FISHER

The UiO-66-NH$_2$ nanoparticles were synthesized according to the previous reports with optimization (Chen et al., 2019; Wang et al., 2017). Specifically, reactions of ZrOCl$_2$·8H$_2$O with NH$_2$-BDC in the presence of acetic acid gave rise to the UiO-66-NH$_2$ nanoparticles. The obtained particles were heated at 80°C under reduced pressure for activation, followed by incubation with PSDC to obtain EV-FISHER.

Transmission electron microscopy (TEM) indicated that the morphologies of UiO-66-NH$_2$ and EV-FISHER were comparable (Figure 2a–b), with the octahedral shapes of UiO-66-NH$_2$ replicated in EV-FISHER, suggesting that PSDC modification has a negligible impact on the MOF structure. Dynamic light scattering (DLS) analysis indicated that the particle size increased from 301 nm for UiO-66-NH$_2$ to 342 nm for EV-FISHER (Figure 2c). Upon decorating with PSDC, the zeta potential also shifted from positive (4.6 mV for UiO-66-NH$_2$) to negative (−21.7 mV for EV-FISHER) due to the negatively charged PO$_4^{3-}$ and DNA (Figure 2d).

In the Fourier transform infrared (FT-IR) spectroscopy of EV-FISHER, there is a new peak of the PO$_4^{3-}$ group at 1049 cm^{-1} as compared to UiO-66-NH$_2$ (Figure 2e). The energy dispersive X-ray (EDX) analysis (Figure 2f) shows the presence of the P element in EV-FISHER. The P 2p peak (134.08 eV) also appeared in X-ray photoelectron spectroscopy (XPS) (Figure S1). The Zr 3d peaks with the binding energy of 185.25 eV and 182.86 eV in UiO-66-NH$_2$ slightly changed to 185.10 eV and 182.74 eV in EV-FISHER (Figure 2g), accountable for its coordination to PO$_4^{3-}$. The absorption peak at 278 nm in the ultraviolet–visible (UV-Vis) spectrum of UiO-66-NH$_2$ slightly blue-shifted to 275 nm with the increased concentrations of PSDC to form EV-FISHER (Figure 2h). In addition, the binding of PSDC could break the ligand to metal charge transfer (LMCT) effect on UiO-66-NH$_2$,
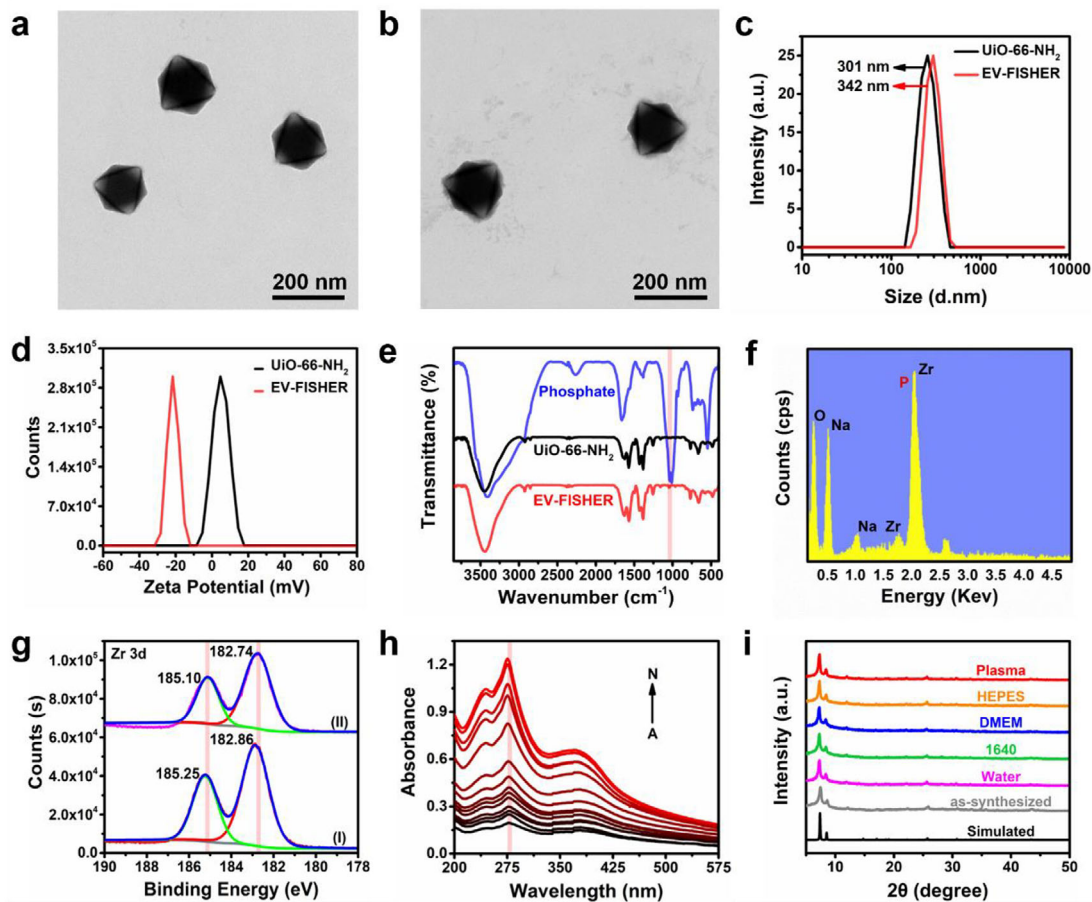
FIGURE 2 Characterization of EV-FISHER platform. TEM images of (a) UiO-66-NH$_2$ and (b) EV-FISHER. (c) The size distribution and (d) zeta potential analysis of UiO-66-NH$_2$ and EV-FISHER, respectively. (e) The FTIR spectra of phosphate (blue), UiO-66-NH$_2$ (black), and EV-FISHER (red). (f) The EDX analysis of EV-FISHER. (g) The XPS patterns Zr 3d peaks in UiO-66-NH$_2$ (I) and EV-FISHER (II). (h) The UV-Vis spectrum for EV-FISHER modified with different concentration of PSDC; (A-N) in the image indicated the concentration of PSDC was 0, 0.1, 0.3, 0.5, 0.7, 0.9, 1.1, 1.4, 1.7, 2.0, 2.5, 3.5, 5.0, 7.0 μM, respectively. (i) The PXRD patterns of UiO-66-NH$_2$ soaked in various solvents

thus recovering its fluorescence (Figure S2) (Yang et al., 2015). The above results collectively authenticated the successful coating of PSDC on the surface of UiO-66-NH$_2$ via the Zr-PO$_4^{3-}$ coordination and thus the reliable construction of EV-FISHER.

Since the stability of EV-FISHER is of great importance during EVs isolation, the structural stability of both UiO-66-NH$_2$ and EV-FISHER were assessed. The powder X-ray diffraction (PXRD) patterns of UiO-66-NH$_2$ immersed in various solvents were in good agreement with the simulated pattern, implying its bulk phase stability (Figure 2i). Moreover, no free ligand NH$_2$-BDC or free Zr(IV) ion was detected in the supernatant from EV-FISHER by mass spectrum (Figure S3) and inductively coupled plasma mass spectrometry (ICP-MS) (Table S4) neither. Additionally, the EV-FISHER showed excellent stability in ultrapure water for 45 days (Figure S4) and exhibited better dispersivity than UiO-66-NH$_2$ in the HEPES buffer (Figure S5). In summary, the prepared EV-FISHER shows sufficient stability to fulfil the requirements of EVs isolation in biological fluids.

3.2 | Characterization of cholesterol-decorated lipid probe

As a lipid probe, PSDC was designed to isolate EVs by inserting cholesterol into the EVs' phospholipid-bilayer membrane. We first investigated this approach at the cell level, as the membrane components of EVs are similar to that of their parent cells. Instead of the PSDC, the fluorophore Cy5 labelled lipid probe Cy5-DNA-cholesterol (denoted as Cy5-DNA-CHO) was employed and incubated with MDA-MB-231 cells for 2 h. As shown in Figure 3(a), the red fluorescence confirmed the successful insertion of the Cy5-DNA-CHO. In contrast, the red fluorescence was absent in the control groups treated with Cy5-DNA, suggesting that cholesterol is a critical component in inducing lipid membrane binding.

The lipid probe Cy5-DNA-CHO and membrane binding were further verified on EVs. The model EVs collected from MDA-MB-231 cells were first incubated with Cy5-DNA-CHO (red fluorescent) and stained with membrane dye PKH67 (green
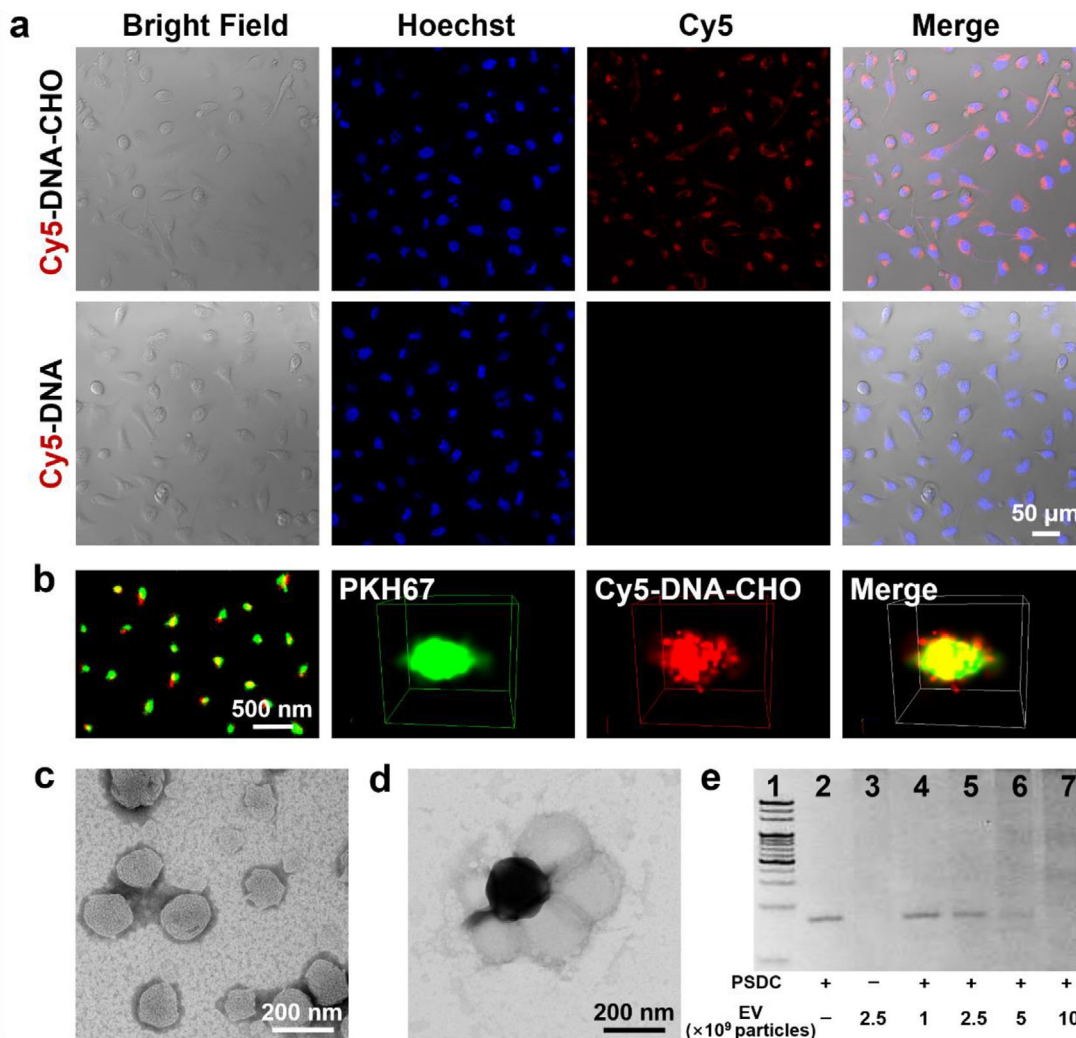
FIGURE 3 Characterization of cholesterol-decorated lipid probe. (a) The confocal images of breast cancer cells MDA-MB-231 treated with Cy5-DNA-CHO and Cy5-DNA, respectively. (b) The lipid probes Cy5-DNA-CHO (red) bind to model EVs (green) derived from MDA-MB-231 cells characterized by super-resolution microscopy. (c) The TEM images of synthesized liposomes with good dispersion and united shape and the (d) Liposomes@EV-FISHER complexes. (e) The SDS-PAGE analysis of the combination between PSDC ($1\,\mu$M) and EVs. Lane 1: marker, lane 2: PSDC only, lane 3: EVs (2.5×10^9) only, lane 4: PSDC + 1×10^9 EVs, lane 5: PSDC + 2.5×10^9 EVs, lane 6: PSDC + 5×10^9 EVs, lane 7: PSDC + 1×10^{10} EVs

fluorescent). Super-resolution imaging pictures depicted excellent co-localization of model EVs (green) and the lipid probes (red) (Figure 3b) with a co-localization ratio of 87% (Figure S6), showcasing efficient recognition of cholesterol towards the EVs membrane. Additionally, EV-like artificial liposomes with negatively charged (Figures 3c and S7) were utilized to mimic the standard EVs consisting of only phospholipid bilayers. The liposomes showed good binding with EV-FISHER (Figure 3d and S8), which indicates the recognition between cholesterol and membrane only involves the phospholipid layer. As demonstrated in sodium dodecyl sulphate-polyacrylamide gel electrophoresis (SDS-PAGE) analysis (Figure 3e), the addition of an increasing concentration of EVs to PSDC (lanes 4–7) showed decreasing bands for the PSDC, and EVs adducts are too large to enter the gel. Taken together, our results confirmed that the lipid probe PSDC is capable of binding to EV membrane.

3.3 | Fishing model EVs with EV-FISHER

We subsequently characterized the feasibility of EV-FISHER for fishing EVs, and the model EVs from MDA-MB-231 cells were used as the source material. Although there were reports on directly capturing peptides or exosomes with MOFs (Chen et al., 2015; Han et al., 2017; Zhang et al., 2020), our findings show that EVs do not attach to the UiO-66-NH$_2$ without decorating PSDC (Figure 4a). On the contrary, model EVs with typical membrane structure (red arrows) can be observed on EV-FISHER (Figure 4b, S9), and similar results were obtained by atomic force microscopy (AFM) as indicated by green arrows (Figures 4c and
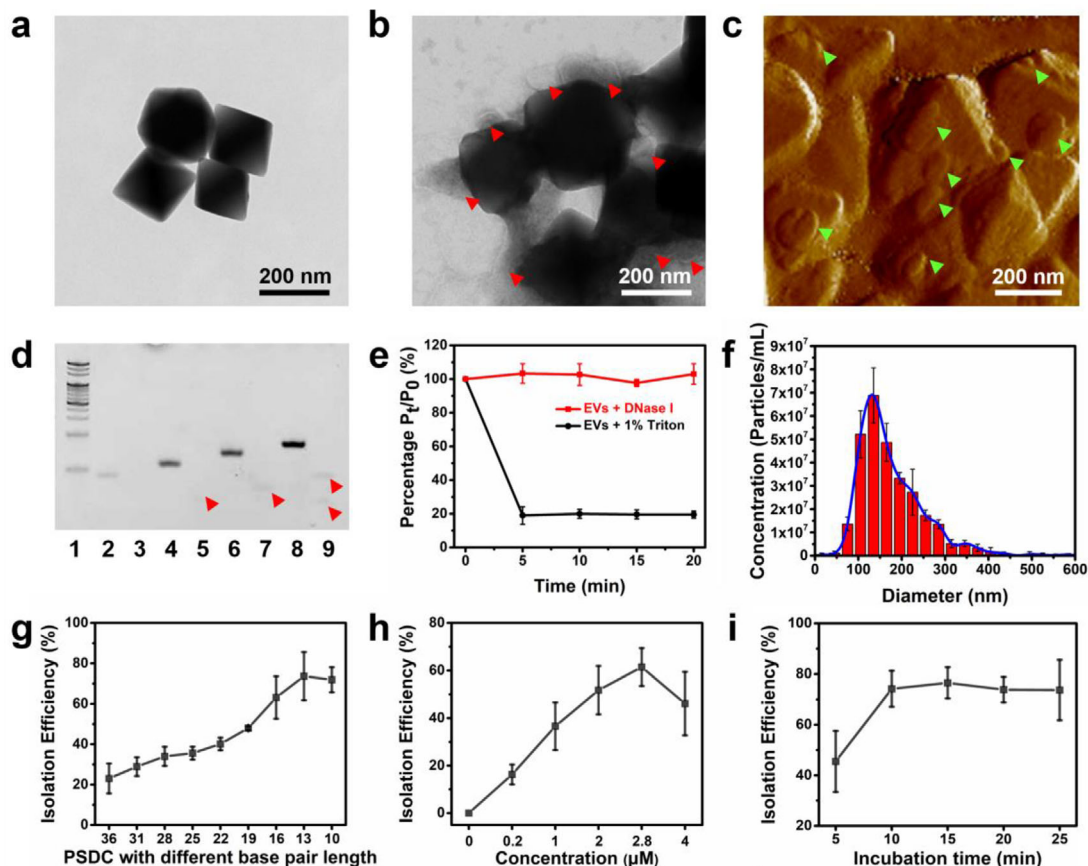
FIGURE 4 Enrichment and isolation of model EVs by EV-FISHER. TEM images of (a) UiO-66-NH$_2$ and (b) EV-FISHER after capturing EVs. The arrows in Figure 4b represent the captured EVs. (c) The AFM image of EVs@EV-FISHER complexes. The arrows in the figure represent the captured EVs. (d) Characterization of the hydrolysis ability of DNase I towards PSDCs by SDS-PAGE; lane 1: marker, lane 2: PSDC7, lane 3: PSDC7 + DNase I, lane 4: PSDC5, lane 5: PSDC5 + DNase I, lane 6: PSDC3, lane 7: PSDC3 + DNase I, lane 8: PSDC1, lane 9: PSDC1 + DNase I. The arrows in the image implied the hydrolysed DNA fragments. (e) EV concentrations after treated with DNase I (red) and Triton X-100 (black) at different time points. (f) Particle counting of model EVs isolated by EV-FISHER. Optimization of the EV-FISHER with (g) PSDC with different base-pair lengths, (h) PSDC8 concentration, and (i) incubation time with EVs ($n = 3$)

S10), implying the successful fishing of EVs. Furthermore, the membrane proteins CD63, CD9, and GPC-1 of the captured EVs were identified as active by immunogold labelling assay (Figure S11). These results demonstrated that EVs maintained structural integrity after being captured by EV-FISHER.

Following the successful EVs fishing, we studied the subsequent release of EVs. As shown in Figure 4(d), DNase I efficiently cleaved PSDC regardless of lengths (PSDC1: 36 bp, PSDC3: 28 bp, PSDC5: 22 bp, and PSDC7: 16 bp) and produced DNA fragments (red arrows). It is also suggested that the EV concentration was hardly affected by DNase I (Figure 4e), while it was distinctly reduced by Triton X-100, indicating DNase I does not affect the integrity of EVs. Furthermore, the captured model EVs were released from the EVs@EV-FISHER system after DNase I treatment (Figure 4f), while no EVs appeared in the control groups (Figure S12). These results confirmed that EV-FISHER could successfully isolate model EVs.

Three significant factors that affect EV's capture and release, including the PSDC length, PSDC concentration, and incubation time, were assessed to improve the isolation efficiency of EV-FISHER. According to the previous reports, the PSDC with long single-stranded DNA might be adsorbed on the surface of UiO-66-NH$_2$, thus losing its mobility and decreasing capturing ability (Yang et al., 2015; Zhang et al., 2014; Zhao et al., 2016). Therefore, PSDC with different lengths (PSDC1, 36 bp) to (PSDC9, 10 bp) (Table S3) were modified on UiO-66-NH$_2$, and the resulting EV-FISHER platforms were named PSDC1@MOF to PSDC9@MOF, respectively. As displayed in Figure 4(g) and S13, the isolation efficiencies were nearly inversely related to the length of PSDC, with the highest rate of 73.7% obtained for PSDC8 (13 bp).

The PSDC density on the UiO-66-NH$_2$ surface was subsequently evaluated using PSDC8. The isolation efficiency gradually improved with the increasing amount of PSDC8, and the best performance was achieved when the concentration of PSDC8 was 2.8 μM. However, the isolation efficiency dropped when the PSDC8 concentration was further increased to 4 μM, presumably due to the steric hindrance (Figure 4h). Therefore, the PSDC8 with a concentration of 2.8 μM was chosen as the optimal concentration
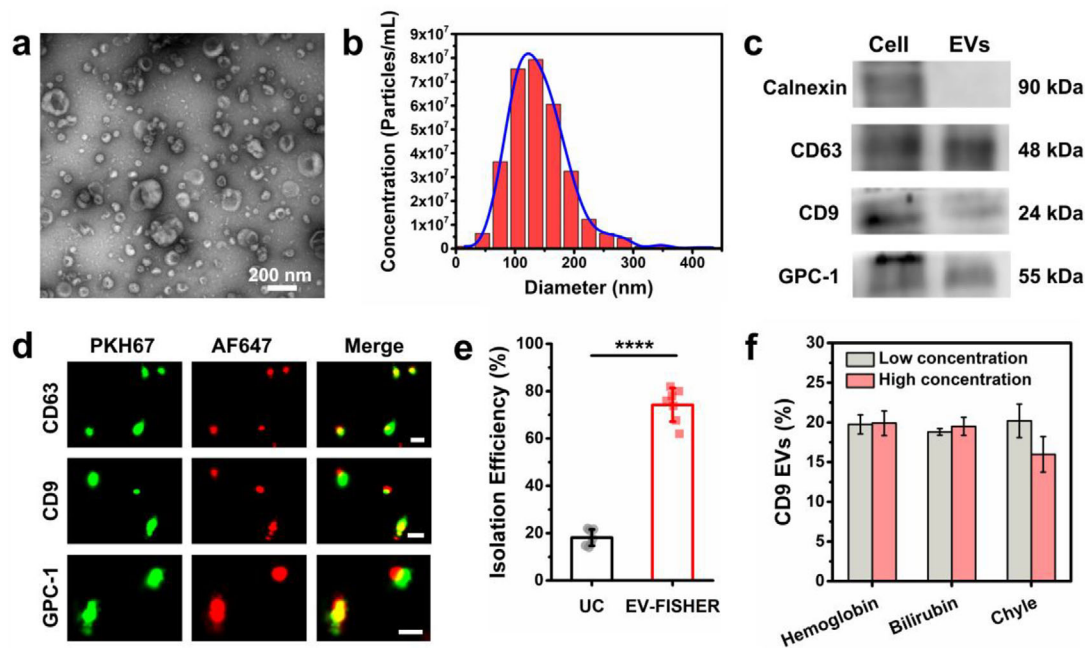
FIGURE 5 Characterization of isolated model EVs by EV-FISHER. (a) TEM images of the isolated model EVs by EV-FISHER. (b) Size distribution of the model EVs isolated by EV-FISHER. (c) The western blot for protein analysis of the model EVs isolated by EV-FISHER. (d) The super-resolution microscopy images of the isolated model EVs (green) labelled with fluorescent antibodies (red) CD63, CD9, and GPC-1, respectively (scale bar: 200 nm). (e) Comparison of isolation efficiency between UC and EV-FISHER using model EVs as source material. (f) The recovery of model EVs isolated by EV-FISHER with the addition of haemoglobin, bilirubin, and chyle, respectively

to rule out the preferred incubation time. Figure 4(i) exhibited that 74.2% of isolation efficiency was obtained at 10 min incubation, and extending incubation time did not hamper or improve the efficiency, implying the EVs fishing was completed at that time.

According to the above results, the mechanism of the efficient isolation performance of EV-FISHER could be elucidated. The surface of EVs is negatively charged, which exhibits weak interaction with the similarly charged molecules. However, the MOF UiO-66-NH$_2$ with positive charge (4.6 mV, Figure 2d) showed almost negligible isolation capacity on EVs (Figure 4a, S12), while EV-FISHER (−21.7 mV, Figure 2d) exhibited high EVs isolation efficiency (Figure 4g). These findings might indicate that EV-FISHER captures EVs mainly depend on the lipid probe PSDC rather than electric charge. Additionally, there were abundant non-EV particles with negative charge within biofluids besides EVs. The negative charge surface of EV-FISHER is expected to reduce the unspecific absorption, thus improving the purity and yield of EVs.

Furthermore, to confirm the universality of the EV-FISHER, another two types of EVs derived from red blood cells (RBC) and fibroblast (L929) were tested. As demonstrated in Figure S14, EV-FISHER can also isolate these two types of EVs with the efficiency of 81.4% ± 3.21% and 69.4% ± 2.88%, respectively ($n = 5$), implying the EV-FISHER should be applicable for EVs from various cell origins.

3.4 | Characterization of the model EVs isolated by EV-FISHER

The model EVs isolated by EV-FISHER showed the classic 'cup shape' membrane structure under TEM (Figures 5a, S15), indicating the isolation process does not damage the integrity. The NTA result revealed that 91.5% of the isolated EVs were within 300 nm with a peak at 123.0 nm (Figure 5b), which was in good accordance with the EVs definition. Furthermore, as expected, three EV markers of CD63, CD9, and GPC-1 were present in the isolated EVs, but not calnexin (a negative control marker) (Figure 5c). Additionally, these proteins (red fluorescence) were identified as active by super-resolution imaging (Figure 5d) with excellent EVs membrane (green fluorescence) colocalization. Besides, the isolated EVs could be effectively taken up and internalized by MDA-MB-231 cells (Figure S16). In summary, EV-FISHER enables the isolation of EVs without damaging their structure and protein components.

The isolation efficacy of EV-FISHER and UC was compared through the model EVs recovery rates. The result showed that EV-FISHER recovered 74.2 ± 7.1% of EVs within an hour, while UC yielded a recovery rate of only 18.1 ± 3.5% after 4 h of laborious processing (Figure 5e), demonstrating the superiority of EV-FISHER in the isolation efficiency, time, and cost. Subsequently, a universal EV biomarker CD9 was employed to validate the quality of EVs isolated by two methods. It was found that a similar
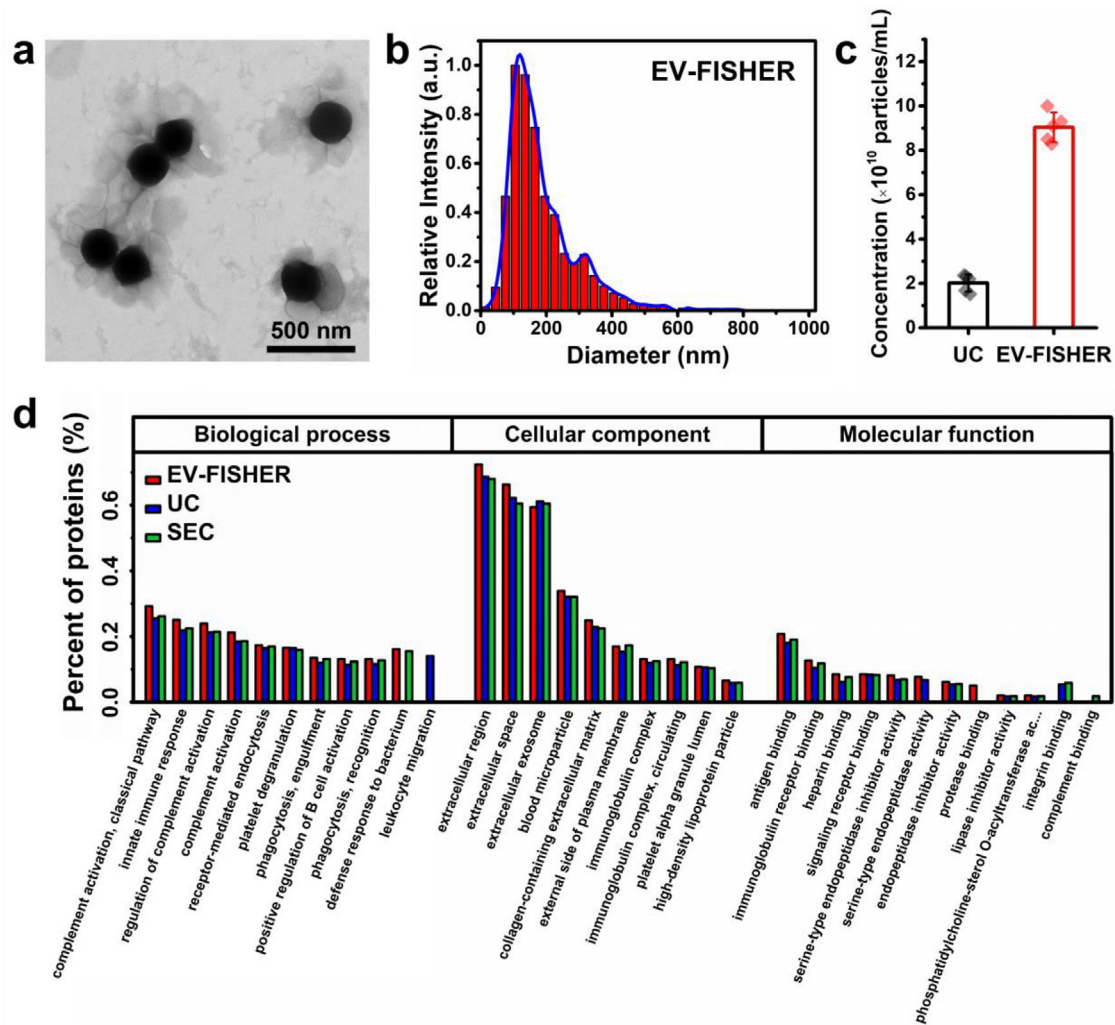
FIGURE 6 Characterization of the plasma EVs isolated by EV-FISHER. (a) TEM image of EV-FISHER capturing EVs from plasma. (b) Size distribution of plasma EVs isolated by EV-FISHER. (c) The concentration analysis of EVs isolated from 1 ml of plasma by UC and EV-FISHER, respectively. (d) Gene Ontology analysis of the peptides from plasma EVs isolated by EV-FISHER, UC, and SEC, respectively

protein ratio was observed in two groups on nano flow cytometer (nFCM) analysis (Figure S17), indicating EV-FISHER has the potential to be a substitute for UC in EV isolation for downstream analysis. In addition, the EV-FISHER proposed a relatively stable isolation efficiency with the coefficient of variation of 7.07% ± 1.77% over 7 days (Figure S18).

Before investigating the practical application, it is necessary to evaluate the anti-interference ability of EV-FISHER. According to the guideline of Interference Testing in Clinical Chemistry (McEnroe et al., 2018) published by Clinical and Laboratory Standards Institute, the model EVs were isolated by EV-FISHER with the addition of three common interferons in plasma, including haemoglobin, bilirubin, and chyle, respectively. Then, the universal biomarker CD9 of the isolated EVs was analysed in different groups by nFCM. As demonstrated in Figure 5(f), there is no difference of CD9 EVs ratio with the addition of haemoglobin (15.0 μM and 25.0 μM, respectively; clinical reference range: < 18.8 μM), bilirubin (10.3 μM and 17.1 μM, respectively; clinical reference range: 3.4−17.1 μM), and low concentration of chyle (2.6 mM; clinical reference range: 0−5.2 mM), while only a slight reduction in the group with a high concentration of chyle (5.2 mM). Therefore, EV-FISHER could potentially isolate EVs in plasma.

3.5 | Fishing plasma EVs with EV-FISHER

Encouraged by the above results, EV-FISHER was employed to isolate plasma EVs. It is shown that EV-FISHER proposed excellent enrichment efficiency toward plasma EVs (Figure 6a). Moreover, the isolated plasma EVs distributed from 15 to 765 nm by NTA (Figure 6b) and the EV markers CD9, CD63 and TSG 101 were also identified (Figure S19). As illustrated in Figure 6(c),
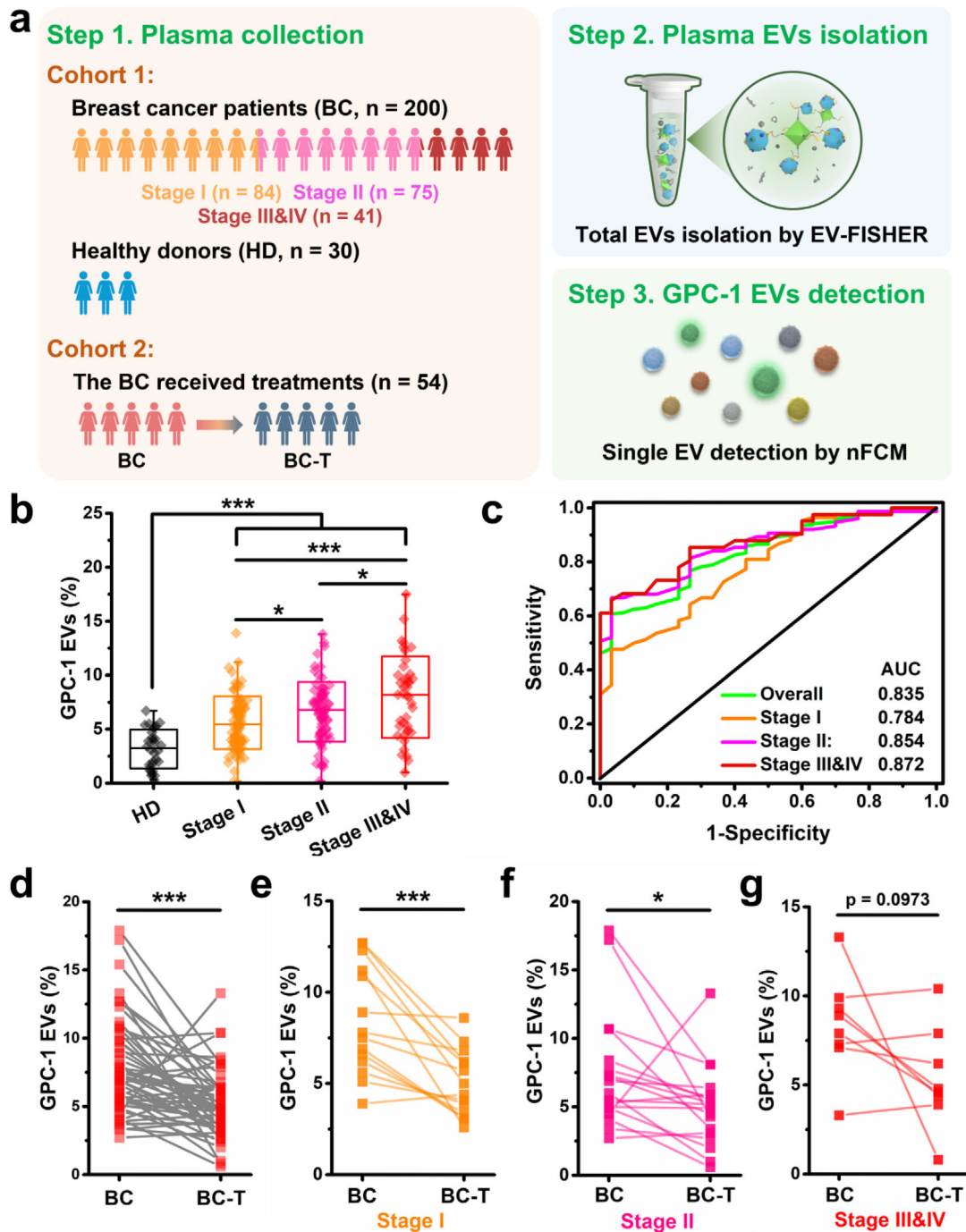
FIGURE 7 Detection of GPC-1 EVs isolated from breast cancer patients and healthy donors. (a) The workflow of breast cancer diagnosis and therapeutic efficacy monitoring includes plasma collection, plasma EVs isolation, and GPC-1 EVs detection. (b) The GPC-1 EVs in healthy donors and breast cancer patients across clinical stages. (c) ROC curve analysis of breast cancer patients with different clinical stages and healthy donors. (d) Dynamic change of GPC-1 EVs in breast cancer patients before and after treatments. Variation of GPC-1 EVs in breast cancer patients with (e) stage I, (f) stage II, and (g) stage III&IV before and after treatments

there were $9.04 \pm 0.68 \times 10^{10}$ EVs particles isolated from 1 ml of plasma by EV-FISHER, which is 4.48 times more than by UC ($2.02 \pm 0.39 \times 10^{10}$), suggesting a better yield of EV-FISHER in practical plasma samples.

Moreover, a 4D label-free proteomic profiling was applied to characterise the plasma EVs isolated by EV-FISHER, using EVs isolated by UC and size-exclusion chromatography (SEC) as references. The results showed that 277, 311 and 309 types of proteins were detected from the EVs isolated by EV-FISHER, UC and SEC, respectively (Supplemental File: 'Protein quantitation', Table S5). All the proteins were at least detected in two isolation methods, suggesting good consistency among EV-FISHER and these

two well-accepted EV isolation approaches (Figure S20). Additionally, the Venn diagram also demonstrated that 247 proteins were identified in all three types of methods (Figure S20), with 79.42% and 79.94% of the proteins from UC and SEC overlapped with EV-FISHER, respectively. It is deduced that the slight diversity of the proteomics results between the three isolation methods might be attributed to the different isolation principles. In addition, 21 out of the top 100 proteins from the *Vesiclepedia* database were identified by EV-FISHER, where 100% and 90.5% were consistent with UC and SEC, respectively. According to the cellular distribution analysis of the identified peptides, EV-FISHER demonstrated similar protein distribution patterns with UC and SEC among three functional regions, including biological process, cellular component, and molecular function (Figure 6d). In addition, according to our proteomic results, there were 15 types of apolipoproteins detected. As shown in Figure S21, the EV-FISHER demonstrated obviously less apolipoprotein contamination than SEC in plasma EVs isolation and exhibited lower apolipoprotein concentration than UC in 10 of 15 apolipoproteins (Table S6 and Supplemental File: 'Protein quantitation'). Therefore, the established EV-FISHER platform displays a better performance over UC and SEC in apolipoprotein elimination during EV isolation from blood.

3.6 | Breast cancer diagnosis and monitoring using plasma EVs isolated by EV-FISHER

The clinical adaptability of EV-FISHER was further studied in clinical cohorts. Firstly, the plasma samples from a breast cancer cohort (Figure 7a, Cohort 1, Table S7 and Table S8) consisting of breast cancer patients (BC) with different subtypes and clinical stages ($n = 200$; that is 84 for stage I, 75 for stage II, 41 for stage III&IV) and healthy donors (HD, $n = 30$) were collected. Next, the plasma EVs were isolated by EV-FISHER, labelled with breast cancer biomarker GPC-1 fluorescent antibody, and conducted single EV analysis on nFCM. As demonstrated in Figure 7(b), a significant analysis of the GPC-1 EVs between healthy donors and breast cancer patients was performed, conforming to the previous report (Melo et al., 2015). It is also found that the GPC-1 EVs in the bloodstream increased from stage I to stage IV, which might be able to utilize as an indicator of breast cancer development. In addition, the receiver operating characteristic (ROC) curves showed an effective classifier with an area under the curve (AUC) of 0.835 to differentiate healthy individuals and breast cancer patients (Figure 7c). Specifically, better diagnostic efficacy was shown for the cancer patients in stage I, stage II, and stage III&IV with the AUC of 0.724, 0.854, and 0.872, respectively.

Additionally, it is reported that the cancer-derived EVs subpopulation of a patient keeps dynamic fluctuation, which could accurately reflect the therapeutic efficacy. Thus, we also collected plasma samples from breast cancer patients before (BC) and after treatments (BC-T) (Figure 7a, Cohort 2, Table S9) for GPC-1 EVs identification. Figure 7(d) depicts a significant reduction in GPC-1 EVs after breast cancer patients underwent treatments, especially for the patients in stages I and II (Figure 7e-f). However, the results showed no statistical difference ($p = 0.0973$) of GPC-1 EVs in the patients in stages III&IV before and after treatments (Figure 7g), which may be accounted for the insufficient cases. Considering the above results, the EV-FISHER is capable of isolating plasma EVs rapidly and efficiently, with good compatibility on downstream single EV subpopulation analysis for clinical cancer diagnostic and treatment efficacy evaluation.

4 | CONCLUSION

In summary, a universal EV isolation platform of EV-FISHER has been constructed based on the lipid probe functionalized UiO-66-NH$_2$. EV-FISHER exhibited merits over UC in terms of its advantages: fast, efficient, and without requiring expensive equipment. The established platform demonstrates the sufficient capability to harvest EVs from plasma in an effective approach. Combining the downstream single EV analysis on nFCM, EV-FISHER enables quick and accurate identification of breast cancer at early stages and provides information on therapeutic efficacy evaluation. Moreover, owing to the delicate design of this isolation strategy, the proposed MOF-based EV isolation platform can be repeated in clinical laboratories with available commercial reagents. This study sheds insights into the design of the clinical applicable EV isolation strategy, promoting the transformation of EV research in liquid biopsy.

CONFLICT OF INTEREST

The authors declare no conflict of interest.

ORCID

Lei Zheng https://orcid.org/0000-0003-2576-8780

REFERENCES

Boriachek, K., Islam, M. N, Möller, A., Salomon, C., Nguyen, N.-T., Hossain, M. S. A., Yamauchi, Y., & Shiddiky, M. J. A. (2018). Biological functions and current advances in isolation and detection strategies for exosome nanovesicles. *Small*, *14*, 1–21.

Chen, L., Yu, F., Shen, X., & Duan, C. (2019). N-CND modified nH$_2$-UiO-66 for photocatalytic cO$_2$ conversion under visible light by a photo-induced electron transfer process. *Chemical Communications*, *55*, 4845–4848.

Chen, Y., Xiong, Z., Peng, L., Gan, Y., Zhao, Y., Shen, J., Qian, J., Zhang, L., & Zhang, W. (2015). Facile preparation of core-shell magnetic metal-organic framework nanoparticles for the selective capture of phosphopeptides. *ACS Applied Materials & Interfaces*, *7*, 16338–16347.

Chen, Y., Zhu, Q., Cheng, L., Wang, Y., Li, M., Yang, Q., Hu, L., Lou, D., Li, J., Dong, X., Lee, L. P., & Liu, F. (2021). Exosome detection via the ultrafast-isolation system: EXODUS. *Nature Methods*, *18*, 212–218.

Choi, D.-Y., Park, J.-N., Paek, S.-H., Choi, S.-C., & Paek, S.-H (2022). Biosensors and bioelectronics detecting early-stage malignant melanoma using a calcium switch-enriched exosome subpopulation containing tumor markers as a sample. *Biosensors Bioelectrons*, *198*, 113828.

Deng, X., Liang, S., Cai, X., Huang, S., Cheng, Z., Shi, Y., Pang, M., Ma, P., & Lin, J. (2019). Yolk-shell structured au nanostar@metal-organic framework for synergistic chemo-photothermal therapy in the second near-infrared window. *Nano Letters*, *19*, 6772–6780.

Doyle, L., & Wang, M. (2019). Overview of extracellular vesicles, their origin, composition, purpose, and methods for exosome isolation and analysis. *Cells*, *8*, 727.

Han, G., Zeng, Q., Jiang, Z., Deng, W., Huang, C., & Li, Y. (2017). Simple preparation of magnetic metal-organic frameworks composite as a "bait" for phosphoproteome research. *Talanta*, *171*, 283–290.

Hu, P.-P., Liu, N., Wu, K.-Y, Zhai, L.-Y., Xie, B.-P., Sun, B., Duan, W.-J., Zhang, W.-H., & Chen, J.-X. (2018). Successive and specific detection of hg^{2+} and I$^-$ by a DNA@MOF biosensor: experimental and simulation studies. *Inorganic Chemistry*, *57*, 8382–8389.

Jackson, K. K., Powell, R. R., Bruce, T. F., & Marcus, R. K (2021). Rapid isolation of extracellular vesicles from diverse biofluid matrices capillary-channeled polymer fiber solid-phase extraction micropipette tips. *Analyst*, *146*, 4314–4325.

Ji, Z., Zhang, H., Liu, H., Yaghi, O. M., & Yang, P. (2018). Cytoprotective metal-organic frameworks for anaerobic bacteria. *Proceedings of the National Academy of Sciences of the United States of America*, *115*, 10582–10587.

Koliha, N., Wiencek, Y., Heider, U., Jüngst, C., Kladt, N., Krauthäuser, S., Johnston, I. C. D., Bosio, A., Schauss, A., & Wild, S. (2016). A novel multiplex bead-based platform highlights the diversity of extracellular vesicles. *Journal of Extracellular Vesicles*, *5*, 29975.

Liang, Y., Lehrich, B. M., Zheng, S., & Lu, M. (2021). Emerging methods in biomarker identification for extracellular vesicle-based liquid biopsy. *Journal of Extracellular Vesicles*, *10*, e12090.

Lin, S.-X., Pan, W.-L., Niu, R.-J., Liu, Y., Chen, J.-X., Zhang, W.-H., Lang, J.-P., & Young, D. J. (2019). Effective loading of cisplatin into a nanoscale uio-66 metal-organic framework with preformed defects. *Dalton Transactions*, *48*, 5308–5314.

Liu, D., Poon, C., Lu, K., He, C., & Lin, W. (2014). Self-assembled nanoscale coordination polymers with trigger release properties for effective anticancer therapy. *Nature Communications*, *5*, 4182.

McEnroe, R., Dimeski, G., Durham, P., Miller, J., Petrides , V., Rheinheimer, D., Smith, M., Warren, K., Zaharik, M. L., & Sonntag, O. (2018). EP07 interference testing in clinical chemistry a guideline for global application developed through the clinical and laboratory standards institute consensus process.

Melo, S. A., Luecke, L. B., Kahlert, C., Fernandez, A. F., Gammon, S. T., Kaye, J., Lebleu, V. S., Mittendorf, E. A., Weitz, J., Rahbari, N., Reissfelder, C., Pilarsky, C., Fraga, M. F., Piwnica-Worms, D., & Kalluri, R. (2015). Glypican-1 identifies cancer exosomes and detects early pancreatic cancer. *Nature*, *523*, 177–182.

Oeyen, E., Van, M. K., Baggerman, G., Willems, H., Boonen, K., Rolfo, C., Pauwels, P., Jacobs, A., Schildermans, K., Cho, W. C., & Mertens, I. (2018). Ultrafiltration and size exclusion chromatography combined with asymmetrical-flow field-flow fractionation for the isolation and characterisation of extracellular vesicles from urine. *Journal of Extracellular Vesicles*, *7*, 1490143.

Tian, Y., Ma, L., Gong, M., Su, G., Zhu, S., Zhang, W., Wang, S., Li, Z., Chen, C., Li, L., Wu, L., & Yan, X. (2018). Protein profiling and sizing of extracellular vesicles from colorectal cancer patients via flow cytometry. *ACS Nano*, *12*, 671–680.

Vasconcelos, M. H., Caires, H. R., Ābols, A., Xavier, C. P. R., & Linē, A. (2019). Extracellular vesicles as a novel source of biomarkers in liquid biopsies for monitoring cancer progression and drug resistance. *Drug Resistance Updates*, *47*, 100647.

Wan, Y., Cheng, G., Liu, X., Hao, Si.-J, Nisic, M., Zhu, C.-D., Xia, Yi.-Q, Li, W.-Q., Wang, Z.-G., Zhang, W.-L., Rice, S. J., Sebastian, A., Albert, I., Belani, C. P., & Zheng, S.-Y. (2017). Rapid magnetic isolation of extracellular vesicles via lipid-based nanoprobes. *Nature Biomedical Engineering*, *1*, 0058.

Wang, B., Wang, P., Xie, L.-H., Lin, R.-B., Lv, J., Li, J.-R., & Chen, B. (2019). A stable zirconium based metal-organic framework for specific recognition of representative polychlorinated dibenzo-p-dioxin molecules. *Nature Communication*, *10*, 3861.

Wang, L., Li, Y., Guan, X., Zhao, J., Shen, L., & Liu, J. (2018). Exosomal double-stranded DNA as a biomarker for the diagnosis and preoperative assessment of pheochromocytoma and paraganglioma. *Molecular Cancer*, *17*, 1–6.

Wang, S., Mcguirk, C. M, Ross, M. B., Wang, S., Chen, P., Xing, H., Liu, Y., & Mirkin, C. A. (2017). General and direct method for preparing oligonucleotide-functionalized metal-organic framework nanoparticles. *Journal of the American Chemical Society*, *139*, 9827–9830.

Wiklander, O. P. B., Brennan, M. Ā., Lötvall, J., Breakefield, X. O., & El Andaloussi, S. (2019). Advances in therapeutic applications of extracellular vesicles. *Science Translational Medicine*, *11*, 1–16.

Woo, H.-K., Sunkara, V., Park, J., Kim, T.-H., Han, J.-R, Kim, C.-J, Choi, H.-I, Kim, Y.-K., & Cho, Y.-K. (2017). Exodisc for rapid, size-selective, and efficient isolation and analysis of nanoscale extracellular vesicles from biological samples. *ACS Nano*, *11*, 1360–1370.

Wu, K.-Y, Chen, M., Huang, N.-H., Li, R.-T., Pan, W.-L., Zhang, W.-H., Chen, W.-H., & Chen, J.-X. (2021). Facile and recyclable dopamine sensing by a label-free terbium(III) metal−organic framework. *Talanta*, *221*, 121399.

Wu, Q., Niu, M., Chen, X., Tan, L., Fu, C., Ren, X., Ren, J., Li, L., Xu, K., Zhong, H., & Meng, X. (2018). Biocompatible and biodegradable zeolitic imidazolate framework/polydopamine nanocarriers for dual stimulus triggered tumor thermo-chemotherapy. *Biomaterials*, *162*, 132–143.

Xie, C., Ji, N., Tang, Z., Li, J., & Chen, Q. (2019). The role of extracellular vesicles from different origin in the microenvironment of head and neck cancers. *Molecular Cancer*, *18*, 83.

Xu, R., Rai, A., Chen, M., Suwakulsiri, W., Greening, D. W., & Simpson, R. J. (2018). Extracellular vesicles in cancer — Implications for future improvements in cancer care. *Nature Reviews Clinical Oncology*, *15*, 617–638.

Yang, J., Dai, Y., Zhu, X., Wang, Z., Y., Zhuang, Q., Shi, J., & Gu, J. (2015). Metal–organic frameworks with inherent recognition sites for selective phosphate sensing through their coordination-induced fluorescence enhancement effect. *Journal of Materials Chemistry A*, *3*, 7445–7452.

Yang, S.-P., Chen, S.-R., Liu, S.-W., Tang, X.-Y., Qin, L., Qiu, G.-H., Chen, J.-X., & Chen, W.-H. (2015). Platforms formed from a three-dimensional Cu-based zwitterionic metal-organic framework and probe ss-DNA: selective fluorescent biosensors for human immunodeficiency virus 1 ds-DNA and sudan virus RNA sequences. *Analytical Chemistry*, *87*, 12206–12214.

Zhang, H., Jiang, W., Liu, R., Zhang, J., Zhang, D., Li, Z., & Luan, Y. (2017). Rational design of metal organic framework nanocarrier-based codelivery system of doxorubicin hydrochloride/verapamil hydrochloride for overcoming multidrug resistance with efficient targeted cancer therapy. *ACS Applied Materials & Interfaces*, *9*, 19687–19697.

Zhang, H., & Lyden, D. (2019). Asymmetric-flow field-flow fractionation technology for exomere and small extracellular vesicle separation and characterization. *Nature Protocol*, *14*, 1027–1053.

Zhang, H.-T., Zhang, J.-W., Huang, G., Du, Z.-Y., & Jiang, H.-L. (2014). An amine-functionalized metal–organic framework as a sensing platform for DNA detection. *Chemical Communications*, *50*, 12069–12072.

Zhang, L., Wang, H., Zhao, G., Li, N., Wang, X., Li, Y., Jia, Y., & Qiao, X. (2021). Anti-Tim4 grafting strongly hydrophilic metal-organic frameworks immunoaffinity flake for high-efficiency capture and separation of exosomes. *Analytical Chemistry*, *93*, 6534–6543.

Zhang, N., Sun, N., & Deng, C. (2020). A hydrophilic magnetic MOF for the consecutive enrichment of exosomes and exosomal phosphopeptides. *Chemical Communications*, *56*, 13999–14002.

Zhang, Y., Wang, F., Ju, E., Liu, Z., Chen, Z., Ren, J., & Qu, X. (2016). Metal-organic-framework-based vaccine platforms for enhanced systemic immune and memory response. *Advanced Functional Materials*, *26*, 6454–6461.

Zhao, H.-Q., Qiu, G.-H., Liang, Z., Li, M.-M., Sun, B., Qin, L., Yang, S.-P., Chen, W.-H., & Chen, J.-X. (2016). A zinc(II)-based two-dimensional MOF for sensitive and selective sensing of HIV-1 ds-DNA sequences. *Analytica Chimica Acta*, *922*, 55–63.

Zhao, X., Wang, Y., Li, D.-S., Bu, X., & Feng, P. (2018). Metal-organic frameworks for separation. *Advance Materials*, *30*, 1705189.

Zhao, Z., Yang, Y., Zeng, Y., & He, M. (2016). A microfluidic exosearch chip for multiplexed exosome detection towards blood-based ovarian cancer diagnosis. *Laboratory Chips*, *16*, 489–496.

Zhu, J., Zhang, J., Ji, X., Tan, Z., & Lubman, D. M. (2021). Column-based technology for CD9-HPLC immunoaffinity isolation of serum extracellular vesicles. *Journal of Proteome Research*, *20*, 4901–4911.

SUPPORTING INFORMATION

Additional supporting information can be found online in the Supporting Information section at the end of this article.